Article

Quantitative Characterization of Age-Related Changes in Peripheral Vessels of a Human Palm Using Raster-Scan Optoacoustic Angiography

Valeriya Perekatova [1,*], **Mikhail Kirillin** [1], **Svetlana Nemirova** [1,2], **Anna Orlova** [1], **Alexey Kurnikov** [1], **Aleksandr Khilov** [1], **Ksenia Pavlova** [1], **Viacheslav Kazakov** [1], **Vadim Vildanov** [3], **Ilya Turchin** [1] and **Pavel Subochev** [1]

[1] Institute of Applied Physics RAS, 603950 Nizhny Novgorod, Russia; mkirillin@yandex.ru (M.K.); nemirova.info@gmail.com (S.N.); ag.orlova@mail.ru (A.O.); kurnikov.1997@ipfran.ru (A.K.); alhil@inbox.ru (A.K.); 780pavlova@gmail.com (K.P.); kazak@appl.sci-nnov.ru (V.K.); ilya340@mail.ru (I.T.); pavel.subochev@gmail.com (P.S.)
[2] Department of Hospital Surgery, Privolzhsky Research Medical University, 10/1 Minin and Pozharsky Sq., 603950 Nizhny Novgorod, Russia
[3] Department of Mathematical Modeling of Economic Processes, State University of Nizhny Novgorod, 23 Gagarina Ave., 603022 Nizhny Novgorod, Russia; kadirovi4@googlemail.com
[*] Correspondence: valeriyaperekatova@gmail.com

Abstract: The analysis of age-related changes in skin vessels based on optoacoustic angiographic images during the in vivo skin monitoring of healthy volunteers at different ages is reported. As a result of a quantitative analysis of the three-dimensional OA images, the age-associated differences in the following image parameters were revealed: image intensity, ratio of blood content at different characteristics depths, total vessel length, and number of branches. The reported approach can be effectively employed for automatic assessment and monitoring of age-related vascular changes in the skin and underlying tissues.

Keywords: optoacoustic angiography; age-related changes in skin vessels; quantitative analysis of blood vessel net

1. Introduction

Age-related changes in peripheral vessels are manifested by a number of structural and functional disorders that reduce the blood supply to tissues, thereby weakening the processes of their gas exchange and hindering the intake of nutrients and the outflow of metabolic products. To date, a number of primary criteria for age-related changes in skin vessels have been identified, which include a decrease in vascular density, violation of branching geometry, a decrease in the number of collaterals, and suppression of vascular reactivity [1]. Similar changes in the peripheral vascular bed can accompany the development of angiopathies common in the population, being a predictor of cardiovascular death [2,3]. Thus, the geometric features of the vessels of different organs in diabetes mellitus are described, and the prognostic value for the development of the disease is shown [4,5]. In atherosclerotic lesions of the arteries, developed collaterals are able to compensate and improve the condition, and a decrease in capillary density is considered a negative prognostic sign [6,7]. Chronic venous diseases with the formation of venous insufficiency are associated with a violation of the architectonics of peripheral vessels, giving positive dynamics in response to adequate therapy [8]. It has been proven that various stages of Raynaud's syndrome, affecting up to 10% of the population [9], is characterized by vasodilation or vasospasm and decreased circulation in the periphery [10,11].

A combination of natural age-related and other pathological changes can mask the true picture of the disease, leading to a late diagnosis. At the same time, vascular dis-

eases significantly increase with the aging of the population [12–15], which also makes it necessary to differentiate the natural age-related changes in angioarchitectonics.

Currently, age-related changes in the microvasculature of surface tissues are studied using both ex vivo and in vivo methods. The method of immunohistochemical analysis with markers of vascular endothelium showed a gradual decrease in the vascularization of human skin with age [16–18]. Decreased capillary loop density and increased vessel length were demonstrated using capillaroscopy and Laser Doppler flowmetry [19,20]. A promising modern method for solving the problem of studying age-related changes in the vascular system of the skin is angiographic optical coherence tomography. This method allowed for the noninvasive identification of age-related decreases in the vessel density and diameter of skin vessels [21], but the visualization depth was up to 350 μm.

Raster-scan optoacoustic (OA) angiography is method being actively developed that is often used to visualize blood vessels, providing optical [22] or acoustic [23] resolution of tens of microns at the imaging depths of several millimeters, which makes it possible to obtain in vivo morphological and functional information on the microvessels' state. However, due to the large amount of 3D data acquired by modern high throughput raster scanning OA systems, the resulting OA vasculature images can be difficult to analyze visually. Therefore, the development of algorithms that extract quantitative information about vessels [24] from OA data is important for analyzing the tissue state.

In this paper, age-related changes in the vascular bed of the skin of healthy volunteers are assessed in vivo for the first time using the OA angiographic technique. As a criterion for analyzing age-related changes in the skin, various parameters of the vascular network of the skin were calculated using a recently developed [25] and successfully applied in [26] algorithm for processing the three-dimensional OA images based on graph representation of the vascular net. The proposed algorithm was used to calculate the parameters characterizing the average density of the vessels, the length of the vessels, and the branching of the vessels on the basis of a graph constructed from a skeletonized image.

2. Materials and Methods

2.1. In Vivo Experiments

In vivo studies were conducted with healthy volunteers 19 to 74 years of age with Caucasian skin (Fitzpatrick type II-III) without confirmed angiopathies, neuropathies, and injuries of the studied areas. The volunteers received no medications during the 3 days prior to the measurement. All studies were carried out under the same conditions; before the start of the investigation, the volunteer was kept the horizontal position for 10 min with a horizontally-located limb. A noninvasive assessment of age-related vascular features of the skin and underlying tissues from the thenar area of both palms was performed. Initially, 8 measurements were taken; however, the images with artifacts (affected by a person's breath, movements, etc.) were excluded by manual selection at the stage of dataset preparation. As a result, for each volunteer, from 2 to 8 measurements were included providing a total of 128 3D images of thenar vasculature. To analyze age-related changes, the volunteers (both female and male) were divided into three age groups: group 1: <35 years ($n = 10$), group 2: 35–49 years ($n = 10$), and group 3: ≥50 years ($n = 10$). All in vivo experiments were approved by the Ethical Committee of Privolzhsky Research Medical University (Protocol #17 from 11 October 2019).

2.2. Raster-Scan Optoacoustic Angiography System

Experimental data were obtained using a custom-made bright-field OA probe (Figure 1) consisting of a polyvinylidene difluoride [27] ultrasonic (US) detector (focal distance F = 6 mm, numerical aperture NA = 0.6, and bandwidth 1–40 MHz) and a multimode optical fiber (diameter 400 μm, NA = 0.22). The scanning OA probe was integrated into an OA microscopy system [28] consisting of a 532 nm laser (pulse repetition rate of 2 kHz, a pulse duration of 1 ns, and a pulse energy of 0.2 mJ) and XY scanning stages (scanning area

of 5×5 mm^2, scanning step 25 μm). The acquisition time for one three-dimensional image was ~5 min.
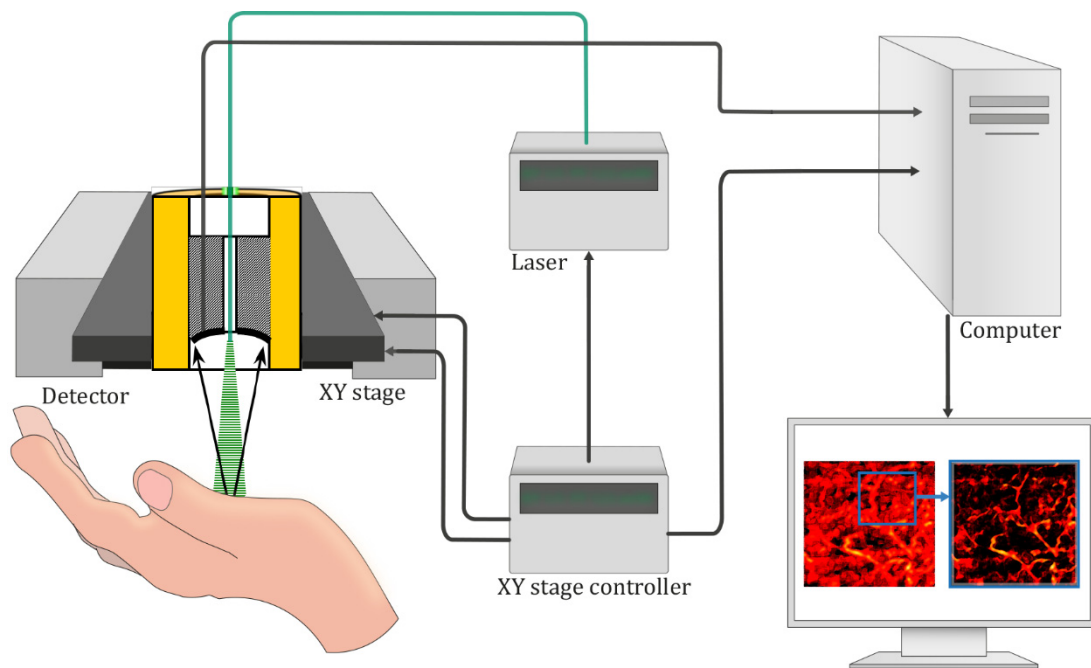

Figure 1. Scheme of OA microscope.

2.3. Quantitative Algorithm for Assessing Vascular Changes

The first stage of the OA image analysis included preprocessing. Two-dimensional delay-and-sum image reconstruction in the frequency domain [29] was applied to the raw OA B-scans in two planes XZ and YZ. The reconstructed 3D images were further Frangi-filtered [30] using the "vesselfilter" function from the k-Wave software package [31]. In the second stage, the quantitative algorithm described in [25] was employed. A mask with a manually selected threshold (the same for all images) was constructed from the Frangi-filtered OA images, converted to binary form, and then skeletonized. A three-dimensional binary voxel skeleton was transformed into a graph [32], characterized by vertices and edges, consisting of "vascular trees" (connected graph structures). The algorithm [25] enabled extraction of the following parameters: the total number of nodes per unit volume, the total number of branches per unit volume, the vessel amount per unit volume (further referred to as "vessel density"), the total length of all vessels per unit volume, rib average length (calculated as the mean distance between two branching points in a blood vessel), and the average length of one vessel. In addition, for a quantitative comparison of the OA images of different age groups, the total intensity over the entire image (further referred to as "image intensity") and the total intensity over the vascular mask (further referred to as "vessel intensity") were calculated. In addition, for each image, the blood content in-depth profile was calculated from the surface to the depth of 2 mm as a ratio of the amount of voxels corresponding to blood vessels at a particular depth to the total number of voxels at this depth.

2.4. Quantitative Algorithm for Assessing Vascular Changes

The obtained quantitative parameters were presented as the average values of each parameter calculated from the OA images and their standard errors of the mean (SEM). The statistically significant differences between age groups were assessed using one-way ANOVA with a posteriori analysis of variance followed by the Duncan's test. Differences were considered statistically significant at $p < 0.05$. Statistical data processing was carried out in Excel and Statistica 12.0 programs.

3. Results and Discussion

Figure 2 shows examples of reconstructed OA images with color-encoded depth (Figure 2a–c), reconstructed en face OA angiograms presented in the projection of the maximum amplitude (Figure 2d–f), and OA sinograms of the palms of healthy volunteers built in the projection of the maximum amplitude onto the surface perpendicular to the scan axis for healthy volunteers from the three age groups: a 24-year-old (Figure 2a,d,g), a 35-year-old (Figure 2b,e,h), and a 69-year-old (Figure 2c,f,i) volunteer. Supplementary Figure S1 provides five more figures for each group. The OA images (Figure 2) demonstrate both small vessels of the superficial vascular plexus of the skin (Figure 2 in purple and orange color) and larger and deeply located vessels (Figure 2 in yellow and green).
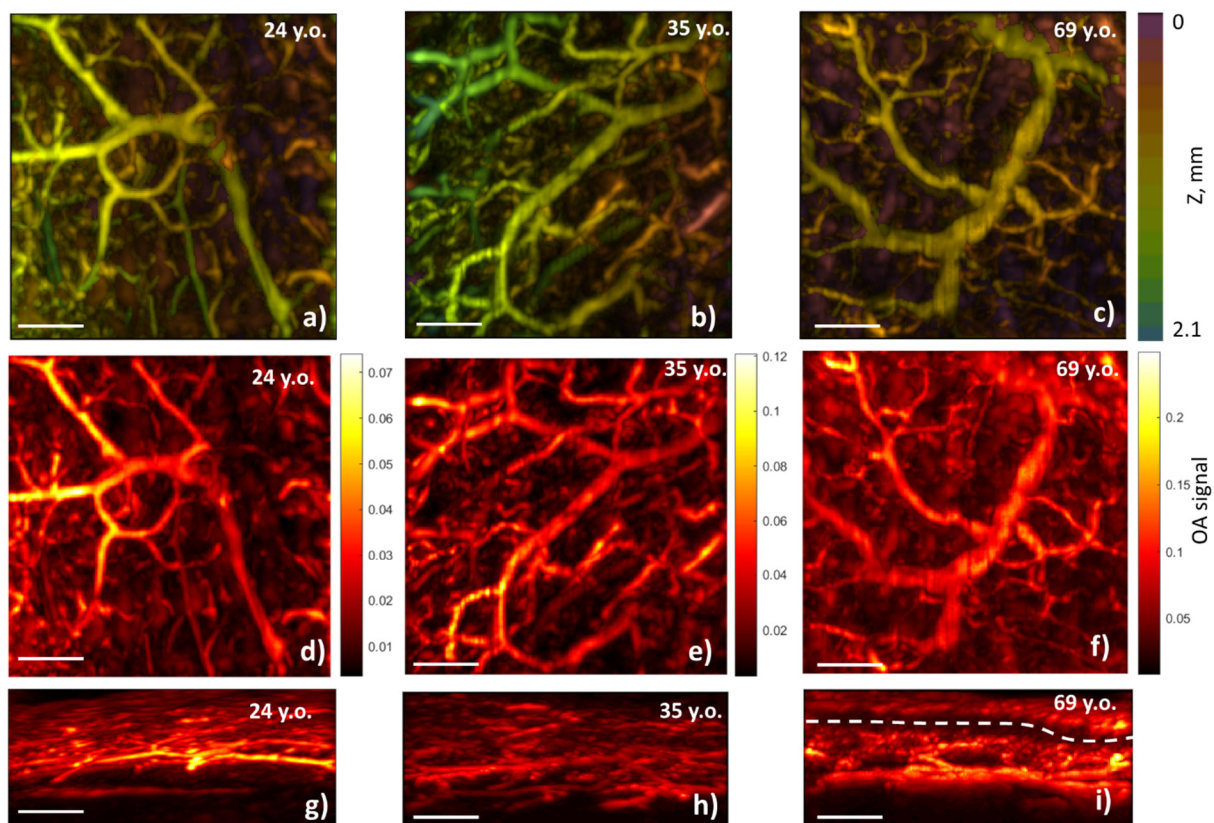

Figure 2. Depth color-encoded OA angiograms (**a**–**c**), OA angiograms (**d**–**f**) built in the projection of the maximum amplitude onto the skin surface of palms and OA sinograms (**g**–**i**) built in the projection of the maximum amplitude onto the surface perpendicular to the scan axis for healthy volunteers from groups 1–3 (24 years old (**a**,**d**,**g**), 35 years old (**b**,**e**,**h**), and 69 years old (**c**,**f**,**i**)). The white dashed line shows the separation of two plexuses. All bars are 1 mm.

In accordance with the modern anatomy paradigm, normal skin microcirculation is organized in two plexuses parallel to the skin's surface. The upper plexus, consisting of small vessels, is located near the papillary dermis. The lower plexus is located at the dermal–hypodermal interface and consists of larger arteries and veins [33]. Figure 2g–i show examples of sinograms (maximum intensity projections, side view) for a volunteer from each of the three groups. From Figure 2i one can see that the two plexuses are clearly separated (the white dashed line in Figure 2i was added for visualization of this separation) for a volunteer from group 3, while for the younger volunteers this separation was not manifested. (Figure 2g,h). In Figure 3a the average blood content in-depth profiles for all three groups are shown together with corresponding SEM ranges. In the superficial layers, the blood content demonstrated a high correlation with age group: group 1 demonstrated low blood content at typical depths up to 300 µm as compared to the lower plexus, while

group 2 demonstrated a comparable value of blood content for both the superficial layers and lower plexus. Group 3 demonstrated two distinguished blood layers separated at a depth of about 300 microns with a pronounced dip of blood content in this area (Figure 3a, red curve). The ratio of blood content at the two characteristic depths $z_1 = 120$ μm and $z_2 = 570$ μm, corresponding to the local maxima of red curve in Figure 3a, demonstrated statistically significant differences between the three age groups and increased with age (Figure 3b).
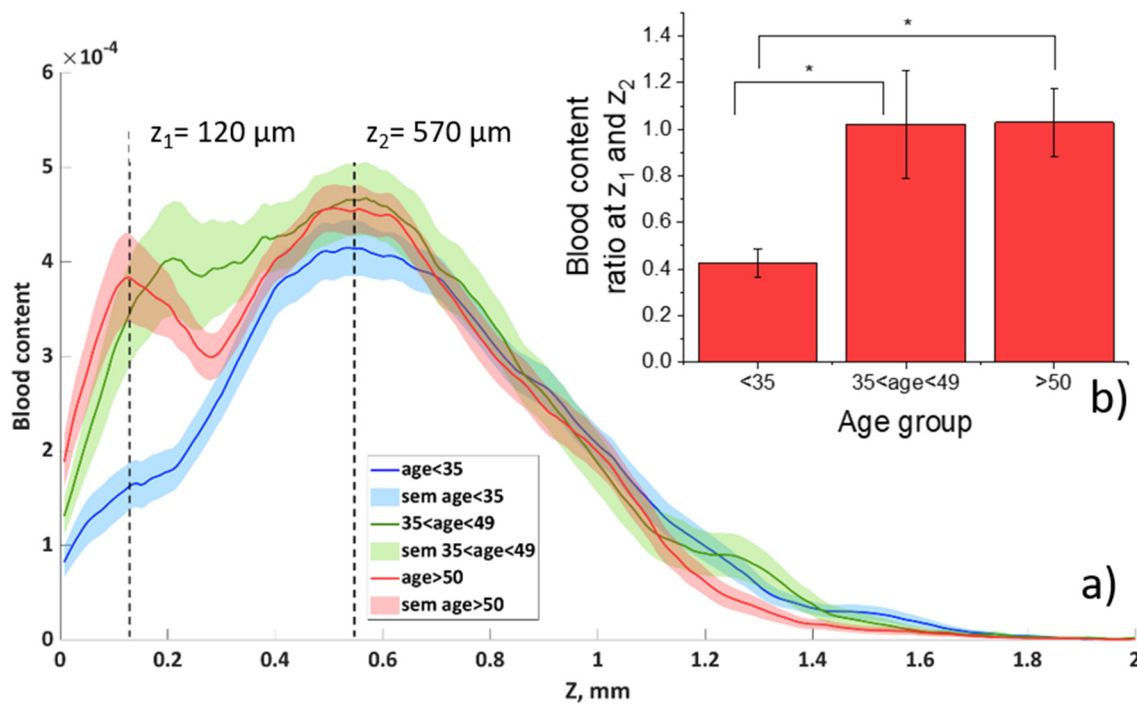

Figure 3. (**a**) Blood content in-depth profiles averaged within each of three age groups (solid lines) with confidence bounds calculated as the standard errors of the mean (SEM) within each group. (**b**) Ratio of blood content at depths 1 and 2 averaged over each age group. The obtained ratios of blood contents are presented as average values and their standard errors of the mean (SEM). Symbol * shows the statistically significant ($p < 0.05$) differences between values in the compared groups.

The reconstructed 3D OA images after the Frangi-filter were used to construct the 3D graphs describing the vascular net. Typical en face OA angiograms presented in the projection of the maximum amplitude (Figure 4a–c) and OA sinograms built in the projection of the maximum amplitude onto the surface perpendicular to the scan axis (Figure 4d–f) with superimposed constructed 3D graphs (white lines) are shown in Figure 4 for the three age groups.

The calculation of the parameters of the vascular network structure was carried out for each 3D data set. Various parameters obtained from the 3D OA angiographic images were averaged over the three age groups; the results are summarized in Figure 5. One can see that the image intensity and vessel intensity increase with age (Figure 5a), while the vessel density decreases with age (Figure 5b). At the same time, the number of nodes in the reconstructed vessel skeleton decreases with age, which can be explained by a decrease in the number of small convoluted vessels.

The corresponding *p*-values (probability values) for the analyzed parameters differences between groups 1, 2, and 3 that were statistically significant ($p < 0.05$) are shown in Table 1.

Statistically significant age-related differences between groups 1 and 3 were revealed in the total intensities summated over the entire image and over the vascular mask only, as well as in the number of branches in blood vessels and total vessel length.
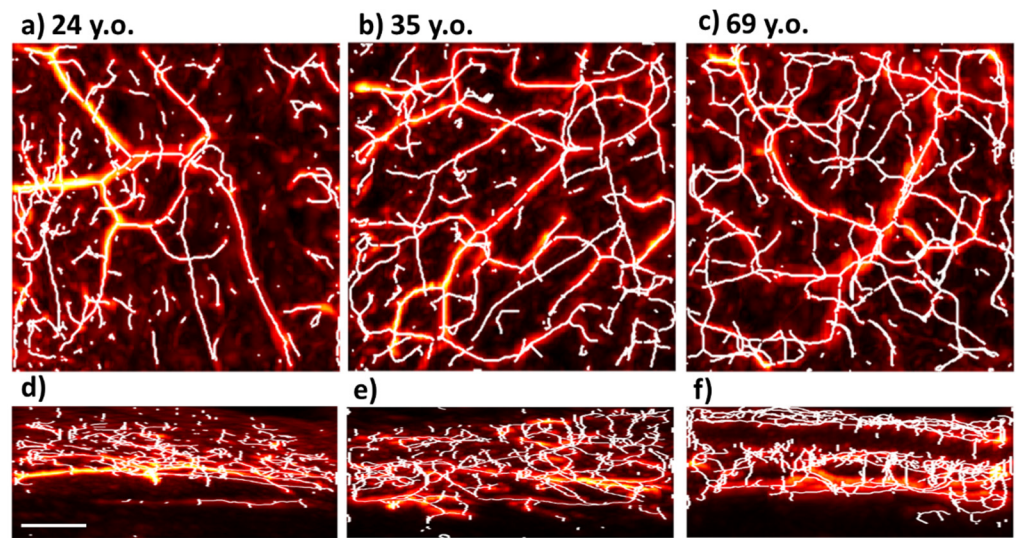
Figure 4. Typical en face OA angiograms presented in the projection of the maximum amplitude (**a–c**) and OA sinograms built in the projection of the maximum amplitude onto the surface perpendicular to the scan axis (**d–f**) with superimposed constructed 3D graphs (white lines) for healthy volunteers from the three age groups: 24 years old (**a,d**), 35 years old (**b,e**), and 69 years old (**c,f**). Bar is 1 mm.

Table 1. Analysis of parameters variance between different groups by the Duncan's test. Differences considered statistically significant ($p < 0.05$) are shown in bold. Group 1: <35 years, group 2: 35–49 years, group 3: ≥50 years. p_{12} is a p-value between group 1 and 2, p_{13} is a p-value between group 1 and 3, p_{23} is a p-value between group 2 and 3.

Parameter	p_{12}	p_{13}	p_{23}
Image intensity	>0.05	**0.002**	>0.05
Vessel intensity	>0.05	**0.000**	**0.012**
Total vessel length	>0.05	**0.026**	>0.05
Number of branches	>0.05	**0.045**	>0.05
Ratio of blood content	**0.041**	**0.004**	>0.05

A decrease with increasing age was revealed for the following parameters: the total number of branches, the total number of nodes, the vessel density, the total length of all vessels, and the average length of one vessel. The average rib length varied insignificantly. The total intensity over the entire OA image in the group of volunteers over 50 years old exceeded that in the group of volunteers < 35 years old by 1.3 times (Figure 5a). The vessel intensity in group 2 was higher than in group 1 by 1.3 times on average, and the values in group 3 were higher than those in group 2 by 1.3 times on average, resulting in a 1.7 times difference between group 1 and group 3. The total vessel length and the number of branching nodes in the group of volunteers over 50 years old were lower than those in the group of volunteers < 35 years old by 1.2 times.

As a result, five parameters showed statistically significant differences between groups 1 and 3: the total intensity over the entire image (Figure 5a) and over the vascular mask (Figure 5a), the total vessel length (Figure 5b), the number of branches (Figure 5d), and the ratio of blood content (Figure 3e). In addition, the total intensity over the vascular mask demonstrated a statistically significant difference between groups 2 and 3, while the ratio of blood content demonstrated a statistically significant difference between groups 1 and 2. Overall, the parameters connected with intensities increased with age, while the indicators characterizing the number of blood vessels decreased with age.

In paper [21], the authors revealed, based on OCT angiography images, that vessel density decreased with age; however, the imaging depth was up to 350 µm limited to the

upper plexus. In this study, the vessel density was calculated in all imaging volume up to 2 mm and was demonstrated to decrease with age (Figure 5c); however, no statistically significant difference was revealed. However, the ratio of blood content between the lower and upper (above 400 μm) plexus demonstrated a statistically significant difference, which was in line with the OCT observations [21]. Color-encoded images (Figure 2) show that the density of the superficial blood vessels decreased with age, which was also consistent with [21]. Deceleration of angiogenesis due to impaired VEGF (vascular endothelial growth factor) signal transmission is considered among the reasons for the decrease in vascular density [1,34]. It is important to note that the gradual decrease in average vessel length and branching with age, revealed in our work, accompanies an increase in the OA signal level. A loss of superficial capillary loops, an increase in the transparency of the skin, and the availability of deep vessels for observation accompanying the aging process [35], inhibition of blood flow, and stasis [36] may be the reasons for the revealed increase in the OA signal level with age.
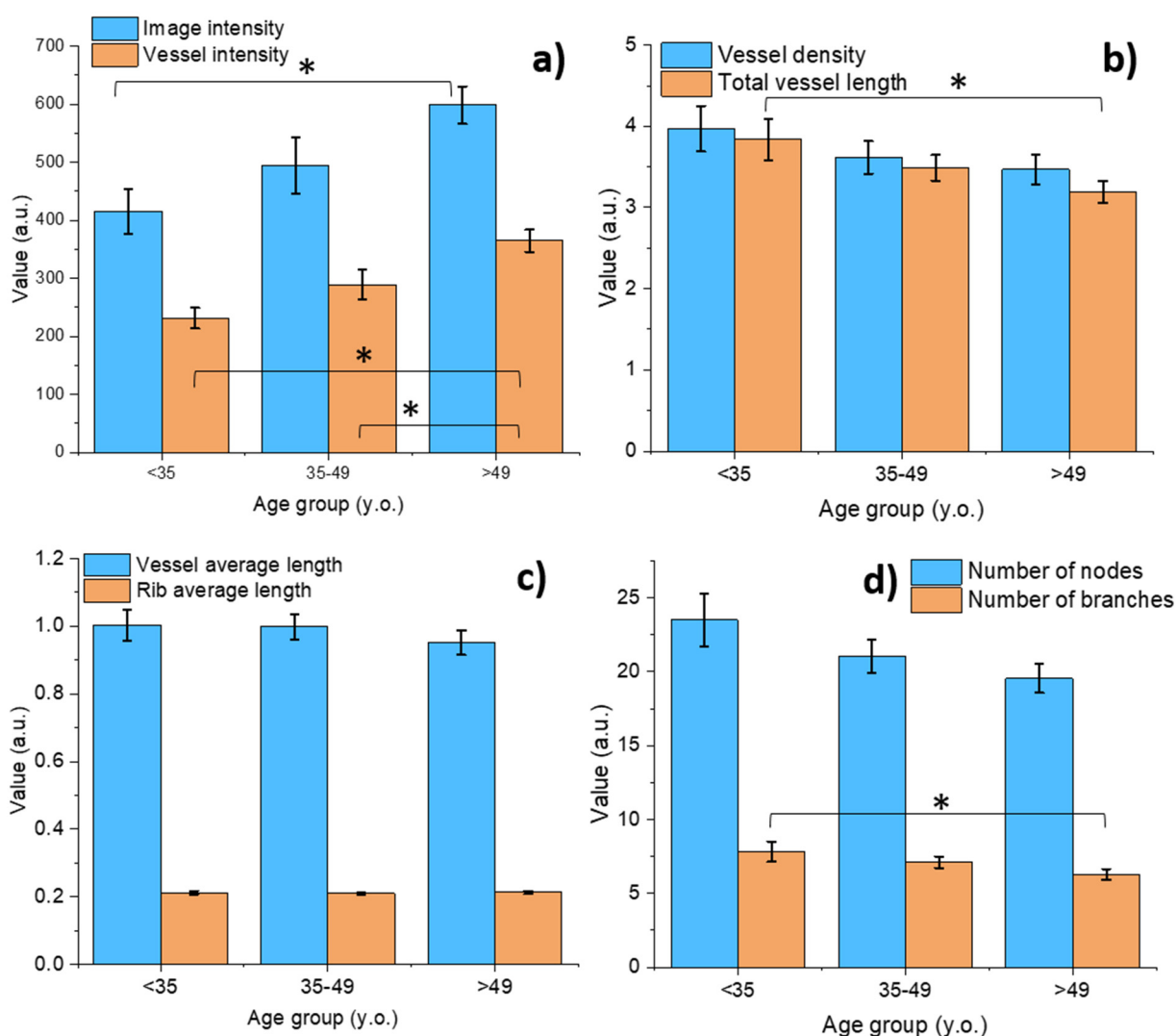

Figure 5. Various parameters were obtained from the OA angiographic images and averaged over each of the three age groups: image and vessel intensity (**a**), vessel density and total vessel length (**b**), vessel and rib average lengths (**c**), number of nodes and branches (**d**). The obtained quantitative parameters were presented as average values and their standard errors of the mean (SEM). Symbol * shows the statistically significant ($p < 0.05$) differences between values in the compared groups.

In this paper, the experiments with Fitzpatrick skin types above III were not performed. Since a recent publication [37] demonstrates certain limitations of OA imaging of deep vessels due to high melanin content in Fitzpatrick skin types IV and V, we expect that a high concentration of melanin in the superficial skin layer could serve as a limitation of imaging deeper vessels and, as a result, to performance of the vessel analysis.

Thus, we can successfully use optoacoustic diagnostics to assess blood vessels in healthy subjects, to monitor premature skin aging, and to identify various stages of angiopathies, in particular chronic venous and arterial insufficiency, regardless of age. In addition, the developed analysis can be used for multispectral OA monitoring of blood vessels, which will allow for verification of arterial and venous pathologies.

4. Conclusions

Age-related changes in the skin of healthy volunteers were analyzed based on OA angiographic images. As a result of the quantitative analysis of three-dimensional OA images based on the skeletonization of the vasculature net, the statistically significant age-associated variations between group 1 (age < 35 y.o.) and group 3 (age > 50 y.o) were revealed for the following parameters: the intensity of the OA images, total vessel length, and number of branches in the vasculature skeleton. In addition, the ratio of blood content at different characteristics depths corresponding to the upper and lower blood plexuses demonstrated a statistically significant difference between group 1 (age < 35 y.o) and groups 2 and 3 (age > 35 y.o.). The proposed algorithm for vasculature analysis can be effectively used for automatic assessment and monitoring of age-related vascular changes in the skin and underlying tissues based on OA diagnostics. In the future, when assessing the state of the vascular architectonics of peripheral tissues, it will be possible to differentiate age characteristics and angio-associated diseases, more reliably assess the severity of the pathological changes, and predict the progression of the disease.

References

1. Bentov, I.; Reed, M.J. The effect of aging on the cutaneous microvasculature. *Microvasc. Res.* **2015**, *100*, 25–31. [CrossRef]
2. Varaki, E.S.; Gargiulo, G.D.; Penkala, S.; Breen, P.P. Peripheral vascular disease assessment in the lower limb: A review of current and emerging non-invasive diagnostic methods. *Biomed. Eng. Online* **2018**, *17*, 61. [CrossRef] [PubMed]
3. Conte, S.M.; Vale, P.R. Peripheral arterial disease. *Heart Lung Circ.* **2018**, *27*, 427–432. [CrossRef] [PubMed]
4. Klein, R.; Lee, K.E.; Danforth, L.; Tsai, M.Y.; Gangnon, R.E.; Meuer, S.E.; Wong, T.Y.; Cheung, C.Y.; Klein, B.E. The relationship of retinal vessel geometric characteristics to the incidence and progression of diabetic retinopathy. *Ophthalmology* **2018**, *125*, 1784–1792. [CrossRef] [PubMed]
5. Alexandre-Heymann, L.; Barral, M.; Dohan, A.; Larger, E. Patients with type 2 diabetes present with multiple anomalies of the pancreatic arterial tree on abdominal computed tomography: Comparison between patients with type 2 diabetes and a matched control group. *Cardiovasc. Diabetol.* **2020**, *19*, 122. [CrossRef]
6. Inampudi, C.; Akintoye, E.; Ando, T.; Briasoulis, A. Angiogenesis in peripheral arterial disease. *Curr. Opin. Pharmacol.* **2018**, *39*, 60–67. [CrossRef]
7. Tibirica, E.; Souza, E.G.; De Lorenzo, A.; Oliveira, G.M. Reduced systemic microvascular density and reactivity in individuals with early onset coronary artery disease. *Microvasc. Res.* **2015**, *97*, 105–108. [CrossRef]
8. Peralta, G.A.; Gardoqui, J.A.; Macías, F.L.; Ceja, V.N.; Cisneros, S.M.; Macías, C.M. Clinical and capillaroscopic evaluation in the treatment of chronic venous insufficiency with Ruscus aculeatus, hesperidin methylchalcone and ascorbic acid in venous insufficiency treatment of ambulatory patients. *Int. Angiol.* **2007**, *26*, 378.
9. Garner, R.; Kumari, R.; Lanyon, P.; Doherty, M.; Zhang, W. Prevalence, risk factors and associations of primary Raynaud's phenomenon: Systematic review and meta-analysis of observational studies. *BMJ open* **2015**, *5*, e006389. [CrossRef]
10. Herrick, A.L. The pathogenesis, diagnosis and treatment of Raynaud phenomenon. *Nat. Rev. Rheumatol.* **2012**, *8*, 469. [CrossRef]
11. Maverakis, E.; Patel, F.; Kronenberg, D.G.; Chung, L.; Fiorentino, D.; Allanore, Y.; Guiducci, S.; Hesselstrand, R.; Hummers, L.K.; Duong, C. International consensus criteria for the diagnosis of Raynaud's phenomenon. *J. Autoimmun.* **2014**, *48*, 60–65. [CrossRef]
12. Blais, C.; Rochette, L.; Ouellet, S.; Huynh, T. Complex Evolution of Epidemiology of Vascular Diseases, Including Increased Disease Burden: From 2000 to 2015. *Can. J. Cardiol.* **2020**, *36*, 740–746. [CrossRef]
13. Youn, Y.J.; Lee, J. Chronic venous insufficiency and varicose veins of the lower extremities. *Korean J. Intern. Med.* **2019**, *34*, 269. [CrossRef]
14. Zhao, Q.; Wang, C.; Guan, S.; Liu, H.; Wu, X.; Liu, C.; Li, H.; Hou, C.; Fang, X. Prevalence characters of peripheral artery disease and associated factors among Beijing residents aged equal and above 35 years old. *Zhonghua Xin Xue Guan Bing Za Zhi* **2019**, *47*, 1000–1004. [CrossRef]
15. Olinic, D.-M.; Spinu, M.; Olinic, M.; Homorodean, C.; Tataru, D.-A.; Liew, A.; Schernthaner, G.-H.; Stanek, A.; Fowkes, G.; Catalano, M. Epidemiology of peripheral artery disease in Europe: VAS Educational Paper. *Int. Angiol. A J. Int. Union Angiol.* **2018**, *37*, 327–334. [CrossRef]
16. Gunin, A.; Petrov, V.; Vasilieva, O.; Golubtsova, N. Age-related changes of blood vessels in the human dermis. *Adv. Gerontol.* **2015**, *5*, 65–71. [CrossRef]
17. Kajiya, K.; Kim, Y.K.; Kinemura, Y.; Kishimoto, J.; Chung, J.H. Structural alterations of the cutaneous vasculature in aged and in photoaged human skin in vivo. *J. Dermatol. Sci.* **2011**, *61*, 206–208. [CrossRef]
18. Quatresooz, P.; Piérard, G.E. Immunohistochemical clues at aging of the skin microvascular unit. *J. Cutan. Pathol.* **2009**, *36*, 39–43. [CrossRef]
19. Li, L.; Mac-Mary, S.; Sainthillier, J.-M.; Nouveau, S.; De Lacharriere, O.; Humbert, P. Age-related changes of the cutaneous microcirculation in vivo. *Gerontology* **2006**, *52*, 142–153. [CrossRef]
20. Kelly, R.I.; Pearse, R.; Bull, R.H.; Leveque, J.-L.; De Rigal, J.; Mortimer, P.S. The effects of aging on the cutaneous microvasculature. *J. Am. Acad. Dermatol.* **1995**, *33*, 749–756. [CrossRef]
21. Hara, Y.; Yamashita, T.; Kikuchi, K.; Kubo, Y.; Katagiri, C.; Kajiya, K.; Saeki, S. Visualization of age-related vascular alterations in facial skin using optical coherence tomography-based angiography. *J. Dermatol. Sci.* **2018**, *90*, 96–98. [CrossRef]
22. Lan, B.; Liu, W.; Wang, Y.-C.; Shi, J.; Li, Y.; Xu, S.; Sheng, H.; Zhou, Q.; Zou, J.; Hoffmann, U.; et al. High-speed widefield photoacoustic microscopy of small-animal hemodynamics. *Biomed. Opt. Express* **2018**, *9*, 4689–4701. [CrossRef]
23. Li, W.; Hofmann, U.; Rebling, J.; Zhou, Q.; Chen, Z.; Ozbek, A.; Gong, Y.; Subochev, P.; Razansky, D.; Dean-Ben, X. Broadband Model-Based Optoacoustic Mesoscopy Enables Deep-Tissue Imaging beyond the Acoustic Diffraction Limit. *Laser Photonics Rev.* **2022**, *16*, 210038. [CrossRef]
24. Corliss, B.A.; Mathews, C.; Doty, R.; Rohde, G.; Peirce, S.M. Methods to label, image, and analyze the complex structural architectures of microvascular networks. *Microcirculation* **2019**, *26*, e12520. [CrossRef]
25. Perekatova, V.; Kirillin, M.; Subochev, P.; Kurnikov, A.; Khilov, A.; Orlova, A.; Yuzhakova, D.; Turchin, I. Quantification of microvasculature parameters based on optoacoustic angiography data. *Laser Phys. Lett.* **2021**, *18*, 035602. [CrossRef]
26. Turchin, I.; Bano, S.; Kirillin, M.; Orlova, A.; Perekatova, V.; Plekhanov, V.; Sergeeva, E.; Kurakina, D.; Khilov, A.; Kurnikov, A.; et al. Combined Fluorescence and Optoacoustic Imaging for Monitoring Treatments against CT26 Tumors with Photoactivatable Liposomes. *Cancers* **2021**, *14*, 197. [CrossRef]

27. Kurnikov, A.A.; Pavlova, K.G.; Orlova, A.G.; Khilov, A.V.; Perekatova, V.V.; Kovalchuk, A.V.; Subochev, P.V. Broadband (100 kHz–100 MHz) ultrasound PVDF detectors for raster-scan optoacoustic angiography with acoustic resolution. *Quantum Electron.* **2021**, *51*, 383. [CrossRef]

28. Subochev, P. Cost-effective imaging of optoacoustic pressure, ultrasonic scattering, and optical diffuse reflectance with improved resolution and speed. *Opt. Lett.* **2016**, *41*, 1006–1009. [CrossRef]

29. Subochev, P.; Spadin, F.; Perekatova, V.; Khilov, A.; Kovalchuk, A.; Pavlova, K.; Kurnikov, A.; Frenz, M.; Jaeger, M. Toward Real-Time Giga-Voxel Optoacoustic/Photoacoustic Microscopy: GPU-Accelerated Fourier Reconstruction with Quasi-3D Implementation. *Photonics* **2022**, *9*, 15. [CrossRef]

30. Frangi, A.F.; Niessen, W.J.; Vincken, K.L.; Viergever, M.A. Multiscale vessel enhancement filtering. In *International Conference on Medical Image Computing and Computer-Assisted Intervention*; Springer: Berlin/Heidelberg, Germany, 1998; pp. 130–137. [CrossRef]

31. Treeby, B.E.; Cox, B.T. k-Wave: MATLAB toolbox for the simulation and reconstruction of photoacoustic wave fields. *J. Biomed. Opt.* **2010**, *15*, 021314. [CrossRef]

32. Kollmannsberger, P.; Kerschnitzki, M.; Repp, F.; Wagermaier, W.; Weinkamer, R.; Fratzl, P. The small world of osteocytes: Connectomics of the lacuno-canalicular network in bone. *New J. Phys.* **2017**, *19*, 073019. [CrossRef]

33. Cracowski, J.L.; Roustit, M. Human skin microcirculation. *Compr. Physiol.* **2011**, *10*, 1105–1154. [CrossRef]

34. Gunin, A.G.; Petrov, V.V.; Golubtzova, N.N.; Vasilieva, O.V.; Kornilova, N.K. Age-related changes in angiogenesis in human dermis. *Exp. Gerontol.* **2014**, *55*, 143–151. [CrossRef]

35. Ryan, T. The ageing of the blood supply and the lymphatic drainage of the skin. *Micron* **2004**, *35*, 161–171. [CrossRef]

36. Waller, J.M.; Maibach, H.I. Age and skin structure and function, a quantitative approach (I): Blood flow, pH, thickness, and ultrasound echogenicity. *Ski. Res. Technol.* **2005**, *11*, 221–235. [CrossRef]

37. Li, X.; Dinish, U.S.; Aguirre, J.; Bi, R.; Dev, K.; Attia, A.B.E.; Nitkunanantharajah, S.; Lim, Q.H.; Schwarz, M.; Yew, Y.W.; et al. Optoacoustic mesoscopy analysis and quantitative estimation of specific imaging metrics in Fitzpatrick skin phototypes II to V. *J. Biophotonics* **2019**, *12*, e201800442. [CrossRef]